Journal of Catalysis 401 (2021) 54–62

Contents lists available at ScienceDirect

Journal of Catalysis

journal homepage: www.elsevier.com/locate/jcat

Surfactant-free colloidal strategies for highly dispersed and active supported IrO_2 catalysts: Synthesis and performance evaluation for the oxygen evolution reaction

Francesco Bizzotto [a], Jonathan Quinson [b], Johanna Schröder [a], Alessandro Zana [a], Matthias Arenz [a,*]

[a] Department of Chemistry, Biochemistry and Pharmaceutical Sciences, University of Bern, Freiestrasse 3, CH-3012 Bern, Switzerland
[b] Chemistry Department, University of Copenhagen, 5 Universitetsparken, 2100 Copenhagen Ø, Denmark

ARTICLE INFO

Article history:
Received 26 January 2021
Revised 7 June 2021
Accepted 4 July 2021
Available online 15 July 2021

Keywords:
Oxygen evolution reaction (OER)
Supported iridium oxide catalysts
Colloidal synthesis
Surfactant-free

ABSTRACT

Water electrolysis is a pivotal technology to drive the energy transition towards a system based on renewable resources. The scarce Ir is a crucial element for the synthesis of heterogeneous catalysts for the oxygen evolution reaction (OER). Carbon supported Ir oxide catalysts obtained from surfactant-free colloidal Ir nanoparticles (NPs) synthesized in alkaline methanol (MeOH), ethanol (EtOH), and ethylene glycol (EG) are investigated and compared. The comparison of independent techniques such as transition electron microscopy (TEM), small angle X-ray scattering (SAXS), and electrochemistry allows shedding light on the parameters that affect the dispersion of the active phase as well as the initial catalytic activity. The colloidal dispersions obtained are suitable to develop supported OER catalysts with little NP agglomeration on a carbon support. Due to the high dispersion of the active phase, initial catalytic activities of more than 400 A g_{Ir}^{-1} are reached at 1.5 V_{RHE} when using carbon as a model support. While the more common surfactant-free alkaline EG synthesis requires flocculation and re-dispersion leading to Ir loss, the main difference between methanol and ethanol as solvent is related to the dispersibility of the support material. The choice of the suitable monoalcohol determines the maximum achieved Ir loading on the support without detrimental particle agglomeration. This simple consideration on catalyst design can readily assist the implementation of more relevant support materials for technical applications and significantly improved catalysts.

1. Introduction

As of today, the majority of the hydrogen used in chemical industry or as fuel in proton exchange membrane fuel cell (PEMFC) powered cars is made from non-renewable resources such as natural gas [1–3]. By comparison, water electrolysis not only can be sustained by renewable energy such as photovoltaic (PV) and wind power, it has the advantage of very high purity. The latter is central to PEMFCs as well as processes such as the Haber-Bosch synthesis of ammonia [4].

However, water electrolysis is characterized by a high total overpotential at the anode process, the oxygen evolution reaction (OER) and, in acidic environment, the anode catalyst consists of precious metals such as Ir and Ru [5–9]. Under these conditions, Ir displays the best compromise between activity and stability as compared to Ru, which exhibits remarkable activity, but degrades quickly. Current commercial anodes for water electrolysis employ a significant amount of Ir, working with loadings of 2 mg_{Ir} cm^{-2} and more, due to the low surface area of these catalysts [10,11]. Therefore, different strategies for the preparation of supported OER catalysts are investigated in this research with the goal to utilize the precious Ir more efficiently. For Pt based PEMFC catalysts, colloidal synthesis strategies have been proven to be an efficient tool for the synthesis of supported catalysts [12–14]. In particular, synthesis procedures avoiding the use of surfactants recently gained momentum since they lead to active catalysts [15,16]. One standard in this respect is the polyol process, mainly using alkaline ethylene glycol (EG) as combined solvent, reducing and colloidal stabilizer agent [17].

In a recent advancement of the colloidal approach, low boiling point solvents could be used as a replacement for EG, in a process we refer to as Co4Cat, leading to readily active catalysts [18]. This new synthesis allowed comparative studies to give new insight into rational catalyst design. In this work, we compare the surfactant-free polyol synthesis (considered as a state-of-the-art

* Corresponding author.
E-mail address: matthias.arenz@unibe.ch (M. Arenz).

https://doi.org/10.1016/j.jcat.2021.07.004
0021-9517/

for surfactant-free Ir NPs synthesis) for the preparation of carbon supported OER catalysts based on Ir NPs with the Co4Cat approach using methanol or ethanol. With carbon as a model support with well-known properties and behavior, we determine the colloidal stability, the size distribution of the NPs on the support employing different precious metal loadings as well as the electrochemical and electrocatalytic properties of obtained OER catalysts. All synthetic routes lead to catalysts with high initial OER activity. However, the results demonstrate the advantages of using low-boiling point mono-alcohols as solvent over the polyol-based route. It is expected that the knowledge gained from our study can help the implementation of oxide-based supports suitable for practical applications.

2. Experimental

2.1. Microwave assisted syntheses of Ir NPs in different solvents: EG, MeOH and EtOH

A microwave-assisted synthesis of Ir nanoparticles (NPs) was performed in three different alkaline solvents, i.e. MeOH, EtOH and EG, following the general procedure previously reported [18]. Typically, 6 mL of a 20 mM solution of $IrCl_3$ (Sigma Aldrich, >99.8 %) in MeOH or EtOH (HPLC grade, Sigma Aldrich) were mixed with 21 mL of a 57 mM solution of NaOH (Suprapur®, Merck) in MeOH or EtOH in a 100 mL round bottom flask connected to a water-cooled condenser. All chemicals have been used as received without further purification. The final concentration of the reaction solution was 4.4 mM of $IrCl_3$ and 44.0 mM of NaOH. The solution appeared yellow at this stage. The flask was then placed into a microwave (MW) reactor (CEM, Discover SP). The reaction was performed under stirring for 30 min while the power of the microwave was kept at 100 W throughout the synthesis. No external cooling was applied during the operation. As soon as the solution approached the boiling point, it turned dark brown, indicating the formation of colloidal NPs.

Ir NP synthesis in EG was performed mixing in a glass vessel 2 mL of a 40 mM solution of $IrCl_3$ in EG together with an equal volume of a 400 mM solution of NaOH in EG. The vessel was then covered with a silicon lid and placed in the MW reactor. The reaction was carried out with the sealed vessel for 3 min up to a set point of 160 °C at a constant power of 200 W with a safety pressure limit of 4 bar. A stream of pressurized air was flushed around the reaction vessel throughout the synthesis to avoid a temperature surge. Once the set point was reached the power was turned off and the vessel was cooled down to room temperature by means of a flow of pressurized air. The colloidal suspension appeared dark brown after the synthesis.

2.2. Preparation of carbon supported catalysts with Ir NPs synthesized in MeOH and EtOH

Supported catalysts have been prepared by dispersing carbon (Vulcan XC72R) in MeOH or EtOH (alcohol to carbon ratio of 2 mL to 1 mg). The suspension was sonicated with a probe sonicator (QSONICA sonicator, 500 W, 50 kHz) for 4 min alternating 1 s of sonication and 1 s of resting. The sonication was performed inside a 15 mL glass vial immersed into water at room temperature to avoid overheating of the suspension. A given volume of Ir NP suspension was then transferred into the vial containing the carbon dispersion while under sonication to avoid agglomeration of the support. This dispersion of carbon and Ir NPs was then sonicated for 10 more minutes. The homogeneous suspension was quantitatively transferred to a 250 mL round bottom flask and the alcohol was slowly evaporated using a rotary evaporator. The round bottom flask was maintained inside a sonication bath throughout the evaporation. Once completely dry, the powder was dispersed in alkaline H_2O/isopropyl alcohol (ratio of 3 to 1 with 1.17 μL of 1 M KOH per 1 mL solution) to obtain a final theoretical concentration of 218 μg_{Ir} mL^{-1} [19].

Supported catalysts with different Ir loadings have been prepared by mixing different ratios of Ir NPs in MeOH or EtOH and carbon suspension in MeOH or EtOH.

Catalysts with a combination of NPs in MeOH and Vulcan XC72R dispersed in EtOH were also prepared. In a typical preparation, a given amount of carbon black was dispered in EtOH with a solvent-to-carbon ratio of 5 mL EtOH per 1 mg Vulcan XC72R. The dispersion was then sonicated with the probe sonicator for 4 min, as described above. Different amounts of Ir NPs dispersion in MeOH were then added to the dispersion to obtain different Ir loadings. All subsequent steps were identical to those employed for the catalysts prepared with pure MeOH and EtOH routes.

2.3. Preparation of carbon supported catalysts with Ir NP synthesized in EG and MeOH including flocculation steps

A given volume of Ir NPs synthesized in alkaline EG sufficient to prepare all Ir/C catalysts (Ir loadings ranging from 10 to 70 wt%) were flocculated from EG by using 1 M HCl. This flocculation step is necessary if EG is used as a solvent to collect and further support the NPs [14]. The volume ratio between HCl and Ir NPs suspension was 2:1. Thereafter the suspension was centrifuged for 10 min at 4500 rpm and the slightly brown supernatant was completely removed and replaced by fresh HCl. The suspension was dispersed again in the sonication bath and centrifuged once more for 10 min at 4500 rpm. The supernatant was again completely removed and acetone added to the Ir NPs to obtain a theoretical concentration of 900 μg_{Ir} mL^{-1}. The Ir NP suspension in acetone was stable and no agglomeration was visible even after several days of storage at room temperature in air. For comparative reasons, to investigate the influence of the flocculation step on the properties of supported catalysts, the same HCl flocculation protocol including redispersion in acetone was also used for MeOH-based NPs (although this flocculation step is not *per se* needed as it is detailed later).

Once the Ir NPs had been precipitated and re-dispersed in acetone, the supported catalysts were prepared by dispersion of carbon in acetone and mixing of the Ir NP suspension in acetone with different Ir-to-carbon ratios followed by extensive sonication. The acetone was thereafter removed by evaporation in a rotary evaporator, as previously described for MeOH and EtOH.

2.4. Transmission electron microscope (TEM) for supported catalysts

The samples for the TEM analysis were prepared by drop casting the diluted catalyst dispersion (about 2 μg_{Ir} mL^{-1}) in MeOH onto carbon coated copper TEM grids (Quantifoil). The size and morphology were estimated by using a Jeol 3000F operated at 300 kV in the case of high resolution (HR) TEM, whereas micrographs of the supported catalysts were recorded with a Tecnai Spirit operated at 80 kV. Micrographs were recorded at different magnifications (at least x240 000 and x300 000) in at least three randomly selected areas.

2.5. ECSA determination by CO stripping

All electrochemical characterization was performed in 0.1 M $HClO_4$ prepared by diluting the concentrated $HClO_4$ (Suprapur®, Merck Germany) with Millipore Milli-Q water (18.2 MΩ cm at 25 °C, total organic content (TOC) of <2 ppb). Ar (99.999%, Carbagas AG, Switzerland) was continuously purged through the electrolyte during the electrochemical experiment.

The electrochemically active surface area (ECSA) of all catalysts was determined *via* CO stripping method prior to any other electrochemical characterization as described in our previous work on unsupported Ir NPs [20]. The electrode was held at 0.15 V_{RHE} in a CO-saturated electrolyte for 20 s. Subsequently, the electrolyte was purged with Ar for 20 min to remove all CO from the solution. The adsorbed CO monolayer was then oxidized to CO_2 by scanning the potential from 0.15 V_{RHE} to 1.4 V_{RHE} at 20 mV s^{-1}. The ECSA was calculated by integration of the oxidation peak and by dividing the as calculated charge by the reference value for polycrystalline Ir of 358 μC cm^{-2} [21].

2.6. Catalyst activation and OER activity determination

Prior to the determination of the OER activity, the catalyst was activated by oxidation at 1.6 V_{RHE} for 300 s and a rotation of 3600 rpm. The electrochemical cell was tilted by an angle of around 30° to improve the detachment of O_2 bubbles from the surface. Once the activation was completed, the potential was lowered to 1.2 V_{RHE}, and subsequently scanned up to 1.6 V_{RHE} at a scan rate of 10 mV s^{-1}. The activity was evaluated based on the current at 1.5 V_{RHE} during the positive going scan. A more detailed description of the activation process alongside the ECSA determination can be found in the work of Bizzotto *et al.* [20].

2.7. Small angle X-ray scattering (SAXS)

SAXS measurements were performed with the SAXSLab instrument at the Niels Bohr Institute, University of Copenhagen, Denmark. The instrument is equipped with a 100XL + micro-focus sealed X-ray tube (Rigaku) producing a photon beam with a wavelength of 1.54 Å. The scattering patterns were recorded with a 2D 300 K Pilatus detector from Dectris. The two-dimensional scattering data were azimuthally averaged, normalized by the incident radiation intensity, the sample exposure time, and the transmission, and corrected for background and detector inhomogeneities using standard reduction software. Liquid samples were placed in sealed quartz capillaries and a background was measured that consisted of the same solvent but without NPs. Powder samples were sealed between two 5–7 μm thick mica windows and measurements were performed in vacuum. The background measurement was bare carbon black Vulcan XC72R. The radially averaged intensity I(q) is given as a function of the scattering vector $q = 4\pi\cdot\sin(\theta)/\lambda$, where λ is the wavelength and 2θ is the scattering angle. The background corrected scattering data were fitted using a power law to take into account the behavior at low q value and a model of polydisperse spheres described by a volume-weighted log-normal distribution.

For the colloidal dispersions the mod the scattering data are fitted to the following expression:

$$I(q) = A\cdot q^{-n} + C\cdot\int P_s(q,R)V(R)D(R)dR$$

where $A\cdot q^{-n}$ corresponds to the power law while A and n are free parameters; C is a scaling constant, and P_s the sphere form factor, V the particle volume, and D the log-normal size distribution. The sphere form factor is given by:

$$Ps(q,R) = \left(3\frac{sin(qR) - qRcos(qR)}{(qR)^3}\right)^2$$

and the log-normal distribution by:

$$D(R) = \frac{1}{R\sigma\sqrt{2\pi}}\exp\left(\frac{-\left[\ln\left(\frac{R}{R_0}\right)\right]^2}{2\sigma^2}\right)$$

where σ is the variance and R_0 the geometric mean of the log-normal distribution.

For the supported NPs, this model alone did not lead to a satisfying agreement between data and fits. The data were best fitted by adding a second model of polydisperse spheres *b* also described by a volume-weighted log-normal distribution with a large distribution that accounts for further background correction. A structure factor contribution was needed to best fit some data. We employed a hard-sphere structure factor F(R,η) as described in Reference [22]. The scattering data are fitted to the following expression:

$$I(q) = A\cdot q^{-n} + C_b\cdot\int P_{sb}(q,R)V_b(R)D_b(R)dR + C\cdot F(R,\eta)\cdot\int P_s(q,R)V(R)D(R)dR$$

C_b is a scaling constant, P_{sb} the sphere form factors, V_b particle volumes, and D_b the log-normal size distribution. The fitting was done using home written MATLAB code to optimize agreement between data and model. The free parameters in the model are: A, n, R_b, σ_b, C_b, R, σ, C, η. More details on the fitting method are described in our previous studies [23,24]. The values obtained for these parameters are reported for Ir NP colloidal dispersions in Table S1 with the corresponding fits in Figure S1. The parameters and relative fits of all supported catalysts are instead reported in Table S2 and Figure S2 respectively. In order to account for the two populations, the reported probability density functions were obtained by weighing the two populations by the relative fraction of surface area of the two populations. The latter was retrieved from the SAXS data as reported in the supporting information (SI).

2.8. Z-Potential measurements

The Z-potential of the colloidal Ir NPs was measured using a Litesizer™ 500 (Anton-Paar) using the software Kalliope Professional (Anton-Paar, version 2.0.1). Measurements were performed in a quartz cuvette at 20 °C (Univette, Anton-Paar). 20 μL of the colloidal Ir NP suspension was transferred into the cuvette and 1 mL of MeOH added to obtain a transmittance of 70–80%. The voltage applied was 40 V whereas 100 runs were performed on each sample. Prior to the measurement, the diluted dispersion was stabilized for around 1 min. All experimental parameters employed can be found in the SI (Table S3) and results in Figure S3 and Table S4.

2.9. Fourier-Transform infrared (FTIR) measurements

The FTIR characterization followed the general procedure previously reported [25]. The final concentration of Ir is ca. 0.5 g L^{-1}. The as-prepared Ir NPs in alkaline (NaOH) MeOH, EtOH and EG were dropped onto a ZnSe crystal for attenuated total reflectance acquisition on a Thermo-Nicolet Avatar 370 FTIR spectrometer. As reference, the same solution as the solvent in which the NPs were redispersed (MeOH, EtOH and EG) was used. All spectra were recorded with a resolution of 4 cm^{-1}.

3. Results and discussion

The full utilization of the precious and scarce material Ir is pivotal for obtaining highly performing OER catalysts. Similar to fuel cell catalysts that are based on Pt, the precious metal utilization of polymer electrolyte membrane water electrolyzer (PEMWE) catalysts can be improved by using supported IrO_2 nanoparticles instead of IrO_2 black. Colloidal approaches are popular to develop Ir-based catalysts [26–28]. Typically, these colloidal approaches to prepare supported catalysts consist of two steps, i.e., first the synthesis of colloidal NPs and second their immobilization onto a support material. Here, we compare different surfactant-free col-

loidal synthesis approaches for the preparation of carbon supported Ir NPs. We first discuss the different synthetic routes to obtain colloidal Ir NPs before we scrutinize the properties of the obtained supported catalysts as well as their electrochemical and electrocatalytic properties for the OER.

3.1. Colloidal synthesis and characterization

Surfactant-free colloidal Ir NPs can be prepared in mono-alcohols with low boiling points such as MeOH and EtOH or with the "higher boiling point" solvent EG. One of the advantages of using mono-alcohols compared to the more traditional polyol synthesis (e.g. using EG) is that "milder" conditions can be applied. The reaction can be performed at 65–75 °C and ambient pressure, whereas the polyol synthesis requires a temperature of about 160 °C. However, a reported benefit of EG is the stability of its colloidal dispersions against flocculation [29,30]. Thus, to evaluate the colloidal stability, the as-prepared Ir NPs synthesized using MeOH and EtOH as solvents have been characterized by their Z-potential, see Table S3. It is found that the colloidal Ir NP suspension prepared in MeOH exhibits a higher absolute Z-potential than the one prepared in EtOH. This finding is consistent with the fact that in MeOH no flocculation is observed even after centrifugation (Figure S4), whereas in EtOH signs of flocculation can be seen after centrifugation. Although the stabilizing mechanism for the Ir NPs was not investigated in the presented work, it should be noted that no surfactant is added to the synthesis medium. Therefore, it is expected that products from the partial solvent oxidation (e.g. CO, see Figure S5) are adsorbed onto the NP surface and thus stabilize the suspension [13,25]. In addition, we have previously demonstrated the importance of OH^- as well as the corresponding cation for the stability of colloidal suspensions [25,31–33]. As pointed out above, Ir NPs synthesized in EtOH are less stable and slightly flocculate after few days of storage, similar to previous reports on the synthesis of Pt NPs in MeOH and EtOH [25]. As already observed for Pt NPs [25], the FTIR band corresponding to the CO stretching mode is significantly weaker in the case of EtOH-based colloidal dispersions (see Figure S5). The lack of adsorbed CO on the Ir NP surface in EtOH might be related to a less facile solvent oxidation to form CO and the formation of different organic side products during the synthesis [25,34]. As mentioned the tendency for EtOH-based dispersions to flocculate fits with the smaller absolute value of the Z-Potential. Nevertheless, sonication effectively redisperses the NPs.

In Fig. 1, we also report the particle size distribution determined by SAXS measurements of the colloidal Ir NPs synthesized in EG, MeOH, and EtOH. The mean particle size of the three different dispersions ranges from 0.8 to 1.1 nm. The differences between the individual values lie within the error of the measurements and thus the particle size distributions can be considered as nearly identical. The tendency of Ir to form such extremely small particles has been previously attributed to its low energy barrier of homogeneous nucleation [35]. Therefore, Ir ions tend to form new seeds rather than growing on preformed ones. Furthermore, it was found in our investigations that Ir behaves differently from Pt in the colloidal synthesis. For the latter, the particle size could be modified by changing the NaOH to Pt ratio (in EG) [13] or by the addition of H_2O (in MeOH) [18]. Moreover, Pt NPs synthesized in alkaline EtOH exhibited a size that depends on the reaction time [25]. For Ir, the obtained particle size was invariant to these factors.

An important advantage of using MeOH or EtOH as solvent is that no flocculation step is required to prepare supported catalysts. The low boiling solvents can be simply evaporated and recovered reducing waste formation [18]. Nevertheless, to obtain non-agglomerated catalysts, the interaction between the active phase and the support as well as the suspension properties of the support in the solvent are critical. Therefore, not only the stability of the Ir colloids has to be considered but also of the support in the respective alcohol [36]. In order to improve the dispersion of the active phase, the contact area between the colloidal NPs and the support should be as high as possible. Consequently, the support should be homogeneously dispersed before mixing it with the colloidal NPs. To highlight this importance, we employed carbon as support material, which has no practical relevance for technical electrolysis, but serves as a model support with well-known properties. We investigated the colloidal stability of the carbon support in the two solvents. As reflected in the Z-potential reported in Table S4 and Figure S3, Vulcan XC72R preferentially disperses in EtOH (lower negative Z-potential value) whereas in MeOH it tends to form flakes of agglomerated carbon particles (see also Figure S6).

The fact that there is no need for a flocculation step is in contrast to the more established procedure using EG as solvent [14,37–39]. In this synthesis, colloidal Ir NPs are first separated from the EG by flocculation before the immobilization step onto the support. This is achieved by mixing with HCl, centrifugation, and redispersion in acetone. In contrast to Pt colloids, during the flocculation of the Ir NPs it is observed that the supernatant remains light brown, suggesting that the NPs cannot be completely flocculated and therefore Ir is partially lost in the process upon the disposing of the supernatant. This would result in a deviation of the actual metal loading on the support from the calculated one, see below where we further investigate the effect of HCl washing. Moreover, when re-dispersed in acetone, the suspension cannot be stored for a long time since Ir NPs seem to dissolve back very slowly to complex species forming a yellow solution, as previously observed for Pt NPs treated in the same manner [30].

	EG	MeOH	EtOH
Particle Size [nm]	0.8 ± 0.2	1.1 ± 0.3	0.8 ± 0.4

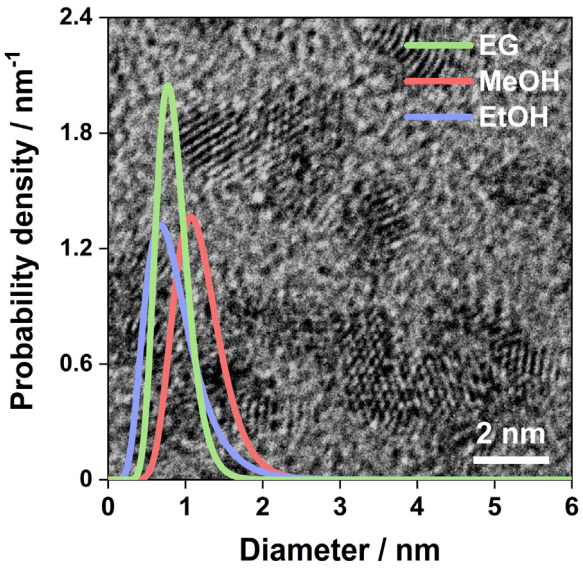

Fig. 1. Upper part: Average particle size determined for freshly synthesized Ir NP prepared in EG (green), MeOH (red), and EtOH (blue). Lower part: Probability densities of the particle size distributions derived from SAXS measurements of the different colloidal suspensions and illustrative HRTEM micrograph of Ir NPs obtained using MeOH. (For interpretation of the references to colour in this figure legend, the reader is referred to the web version of this article.)

Table 1
Mean diameter in nanometers determined by SAXS. Ir/C catalysts prepared with Ir NPs synthesized in EG, MeOH and EtOH are characterized. For each solvent, the series of different metal loadings was prepared from the same batch of Ir NPs. Four different loadings were targeted, i.e. 10, 30, 50, 70 wt%. The error in the particle size distribution corresponds to the variance of the log-normal distribution employed in the fitting of SAXS data.

Ir/C	10 wt%	30 wt%	50 wt%	70 wt%
EG	2.0 ± 0.3	2.0 ± 0.3	1.8 ± 0.3	1.9 ± 0.3
MeOH	1.9 ± 0.3	1.8 ± 0.3	1.8 ± 0.3	1.7 ± 0.5
EtOH	2.0 ± 0.3	1.8 ± 0.4	1.8 ± 0.4	1.9 ± 0.5

3.2. Preparation of supported catalysts from colloidal Ir NPs with different solvents

In the next step, for each solvent (EtOH, MeOH, and EG) a series of Ir/C catalysts with different metal loadings, i.e., 10, 30, 50, 70 wt % was prepared. We then determined the mean nanoparticle diameter of the different supported catalysts *via* SAXS. One of the main challenges of the synthesis of supported catalysts is to uniformly coat the entire surface of the chosen support with particles even at high metal loading. Such a complete coating is beneficial for the long-term stability as well as the electronic conductivity of the catalyst [40]. The values reported in Table 1 show that nearly identical average particle sizes are found for all catalysts, i.e. ca. 2 nm in diameter. The result demonstrates the strength of the colloidal approach enabling the use of the same NP stock suspension to prepare a series of supported catalysts with the same particle properties. It should be mentioned, however, that despite the identical average particle size, depending on the solvent the size distribution tends to broaden slightly with increasing metal loading indicating minor particle agglomeration.

Interestingly, the carbon supported Ir NPs prepared in EG (Ir/C_{EG}) display the narrowest size distribution for all metal loadings. It is however important to bear in mind that the flocculation step that is required for EG does not lead to a quantitative transfer of Ir NPs to acetone. The immediate consequence is a lower actual mass loading that might result in lower agglomeration.

TEM micrographs allow shedding light on the trends in agglomeration that were hinted at by SAXS. For Ir/C_{EtOH}, the NPs are homogeneously dispersed on the support in all investigated samples (Figure S7, EtOH). Especially at 10 and 30 wt% loadings, the NPs are evenly spaced by several nanometers with only a few spots that display slight aggregation. The Ir/C_{MeOH} samples instead exhibit good dispersion only at lower metal loadings (10 and 30 wt%, Figure S8). Already at 50 wt% the NPs appear less homogeneously distributed on the support but the quality of the catalysts is still comparable to the EtOH-based catalysts. For Ir/C_{EG}, at metal loading of 50 wt% the dispersion is rather good, with no visible agglomeration (Figure S9).

However, when the metal loading is increased to 70 wt% the influence of the solvent becomes apparent. The difference in particle agglomeration of the supported catalysts is demonstrated by comparing the respective catalysts with 70 wt% metal loading on the carbon support using TEM, see Fig. 2. For Ir/C_{EG}, it can be observed that although the Ir NPs are homogeneously distributed on the carbon black and almost completely covering it, some areas of the support can be identified that are uncovered by NPs, such as the one in the center of Fig. 2a. Clear particle agglomeration can be observed for Ir/C_{MeOH} with 70 wt% metal loading, see Fig. 2b. Several "free spots" are discernable on the carbon support, whereas some Ir NPs formed thick aggregates. This poor dispersion we typically observed in Ir/C_{MeOH} is in contrast to Ir/C_{EtOH} with high metal loading. As displayed by Fig. 2c, the carbon black support is entirely covered with Ir NPs that assemble in a packed but thin layer of NPs under which the morphology of the support is still perfectly visible. Considering the Z-potential measurements, a possible explanation for the observed behavior lies in the dispersion of the carbon support in the respective solvents rather than on the colloidal

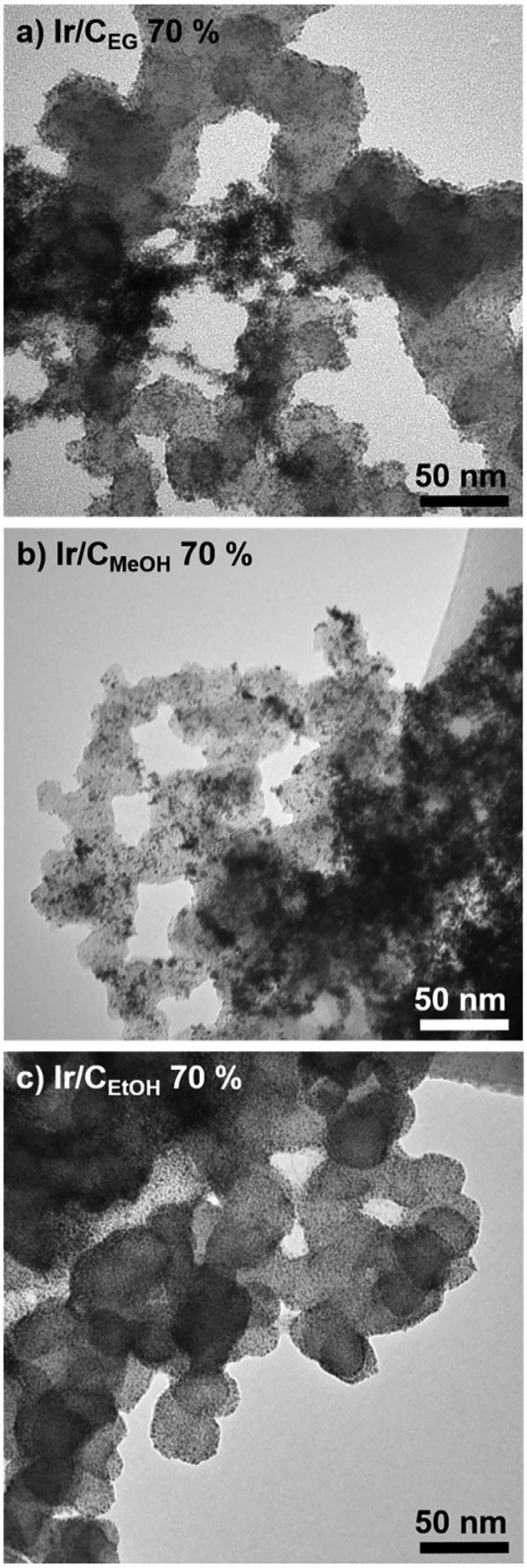

Fig. 2. TEM micrographs taken at 300 000x magnification on Ir/C 70 wt%. The solvents employed for synthesis and dispersion of carbon flakes are a) EG, b) MeOH, and c) EtOH. The scale bar is set for all micrographs to 50 nm.

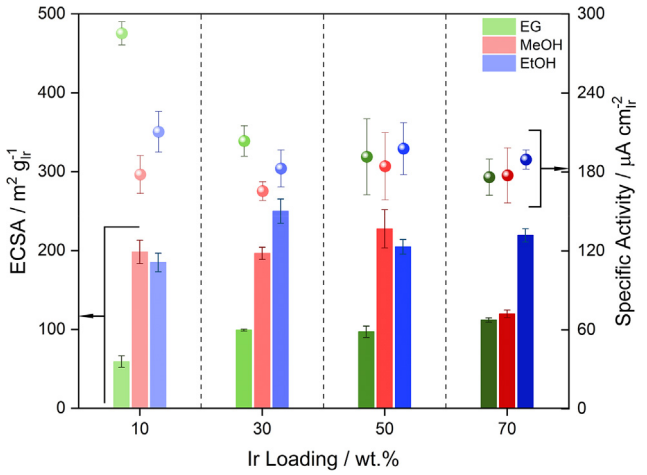

Fig. 3. Electrochemical characterization of Ir-based catalysts prepared with metal loadings of 10, 30, 50, 70 wt%. Columns display the ECSA measured with the CO stripping method (left axis), whereas dots the specific activity (SA) measured after normalization by the roughness factor (RF) of the geometric current (right axis). SA has been measured at 1.5 V_{RHE} during the first positive going scan following catalyst activation at 1.6 V_{RHE}. Scan rate of 10 mV s^{-1}, potential range 1.2 – 1.6 V_{RHE} and temperature 298 K.

Table 2
Mass activity (MA) of Ir-based catalysts prepared with metal loadings of 10, 30, 50, 70 wt%. All catalysts have been measured in Ar-saturated 0.1 M $HClO_4$ solution at 1.5 V_{RHE} during the first positive going scan following catalyst activation at 1.6 V_{RHE}. Scan rate of 10 mV s^{-1}, potential range 1.2–1.6 V_{RHE}, and temperature 298 K. All currents have been normalized by the theoretical total Ir mass loading of 1.96 µg.

Ir Loading [%]	MA - EG [A g_{Ir}^{-1}]	MA - MeOH [A g_{Ir}^{-1}]	MA - EtOH [A g_{Ir}^{-1}]
10	168 ± 16	348 ± 11	388 ± 14
30	201 ± 11	304 ± 6	456 ± 21
50	185 ± 24	342 ± 30	405 ± 36
70	197 ± 15	212 ± 24	415 ± 2

stability of the Ir NPs. Based on their Z-potential and the visual evaluation for flocculation, Ir NPs are more stable in MeOH than in EtOH. However, the carbon support is significantly better dispersed in EtOH as compared to MeOH (Fig. 2 and Figure S6). It can therefore be concluded that the stability of the support in the solvent prior to the NP immobilization is at least as critical for achieving high metal loadings without agglomeration as the colloidal NP stability, see also discussion below where the ECSA determined for catalysts prepared by mixing carbon dispersed in EtOH and Ir NPs synthesized in MeOH is investigated. In the case of lower metal loading, the NP dispersion on the support is comparable using EtOH or MeOH as solvent (see Figure S7 and S8 respectively).

3.3. Electrochemical and electrocatalytic characterization

A complementary approach to investigate the dispersion of the Ir NPs on the carbon support is to determine their ECSA. A complete electrochemical characterization of the catalysts was carried out to study the effect of the metal loading on their electrochemical and catalytic (OER) properties. For each catalyst, we measured the ECSA with the CO stripping method, and after activation, the specific activity (SA) for the OER from the geometric current density and the roughness factor (RF). We carefully chose the potential range for the CO stripping to guarantee a quantitative conversion of the CO to CO_2 and avoid undesired oxidation of the carbon support. Furthermore, the mass activity (MA) for the OER was determined by considering the nominal Ir loading, i.e. 10 μg_{Ir} cm^{-2}, on the rotating disk electrode (RDE) tip (see Fig. 3 and Table 2). A more complete table with all electrochemical results can be found in the SI (Table S5). The CVs recorded during the CO stripping procedure and the OER investigation are reported in the SI (Figure S10).

We begin the discussion with Ir/C_{EG} which can be regarded as a reference as the synthesis and characterization is similar to the well-established Pt/C_{EG} catalysts [12,17,41]. The nominal ECSA is found to be around 100 m^2 g_{Ir}^{-1} for all samples except the 10 wt% for which a nominal ECSA of 60 m^2 g_{Ir}^{-1} is determined. The SA of the OER is found to be independent of the metal loading for 30, 50, and 70 wt% for which activities of ca. 180 µA cm_{Ir}^{-2} were determined. However, for 10 wt% the determined SA is significantly higher, i.e., 280 µA cm_{Ir}^{-2}.

However, the MA is relatively constant within the experimental uncertainty, i.e., 180 – 210 A g_{Ir}^{-1} for all catalysts. This finding is at first sight surprising. Considering that the SA was calculated from the RF and the ECSA determined for the 10 wt% sample is surprisingly low, it can be assumed that this finding is in fact a consequence of an underestimation of the ECSA. As the CO stripping method requires metallic Ir, such underestimation could be due to an irreversible oxidation of the NPs [20]. This phenomenon would also explain the relatively small ECSA values determined in previous work [15]. In a recent publication that investigated the degradation of Pt NPs synthesized in EG and deposited on carbon black it was also observed that at low metal-to-carbon ratios the oxidation state of the Pt was higher [42]. Differently from Pt, Ir cannot be electrochemically reduced in the potential range here investigated. Therefore, a partially oxidized Ir would lower the amount of CO that could adsorb on the surface and consequently the measured ECSA.

The MeOH-based catalysts are instead characterized by a substantially higher ECSA, i.e., 195–230 m^2 g_{Ir}^{-1} in the loading range of 10–50 wt%. We attribute this significant deviation with respect to Ir/C_{EG} to a loss of Ir during the flocculation step performed with HCl in agreement with the fact that the supernatant in the flocculation step remains light brown, see also below. Such substantially higher values of ECSA fit with the small size of the NPs. For NPs having a diameter of 0.9 nm, and assuming a spherical shape, the maximum expected ECSA should be around 300 m^2 g_{Ir}^{-1}. The surface of the NPs is however not entirely available due to the contact between the NP and the support. Such contact area is generally approximated to 30% of the total area, decreasing the maximum ECSA to around 210 m^2 g_{Ir}^{-1}. However, it is important to bear in mind that this is only an estimate and different models may lead to significantly higher values of maximum theoretical ECSA [43]. The Ir/C_{MeOH} 70 wt% catalyst sample exhibits a substantially lower ECSA as well, i.e. only 119 m^2 g_{Ir}^{-1}. Here, agglomeration of Ir is the most probable cause in line with the observed agglomeration in the TEM and SAXS analyses. This means, that only for the samples where Ir is homogeneously dispersed on the support and a narrow size distribution is obtained, high utilization of the Ir is achieved.

The SA, however, is unaffected by the agglomeration and is constant within the accuracy of the measurements ranging from 165 to 185 µA cm_{Ir}^{-2}. Considering that the SA is constant for all loadings, the MA must follow the same trend of the ECSA, with a significant drop in the activity at 70 wt%. Up to 50 wt%, the MA achieves values as high as 305–350 A g_{Ir}^{-1}, whereas "only" 212 A g_{Ir}^{-1} are determined for the Ir/C_{MeOH} 70 wt% catalyst. It should be stressed that this is still an outstanding performance, considering that state-of-the-art Ir-based catalysts typically exhibit surface areas in the range of 10–60 m^2 g_{Ir}^{-1} and MA values lower than 200 A g_{Ir}^{-1} even at low Ir loading [27,44–51].

In the attempt to account for the lower ECSA and MA of EG-based catalysts, we also tested the influence of the flocculation step

by comparison of a standard Ir/C_{MeOH} 50 wt% and Ir/$C_{MeOH,\ HCl}$ 50 wt% (see Table S6 and Figure S11). In the latter case, Ir NPs suspended in MeOH were precipitated with 1 M HCl and then redispersed in acetone before the immobilization step; i.e. the same procedure used in the polyol synthesis. Determining the ECSA and MA by assuming that all Ir NPs have been precipitated, the values decrease by around 40 % compared to the standard Ir/C_{MeOH} sample (see Table S6). Given that neither in the TEM nor in the SAXS data displayed in Figure S11 particle agglomeration is apparent, we attribute this difference to a partial loss of NPs during the flocculation. Considering the extremely low abundance of Ir, such loss in the catalyst synthesis would not be acceptable for any applications. The absence of Ir loss also highlights the advantages of using low boiling point solvents that do not require any flocculation step.

The best performance is achieved for the EtOH-synthesis-based catalysts. In the low loading range, the ECSA is comparable to the MeOH-based catalysts, i.e., from 185 $m^2\ g_{Ir}^{-1}$ of 10 wt% up to 250 $m^2\ g_{Ir}^{-1}$ for the 30 wt%. The most striking result, however, is the ECSA of the 70 wt% catalyst which is still as high as 220 $m^2\ g_{Ir}^{-1}$. This suggests that no significant agglomeration took place during the supporting step, as is also suggested by the SAXS and TEM data. The determined SA is slightly higher than for the MeOH-based catalysts and constant for all metal loadings, i.e., 180–210 $\mu A\ cm_{Ir}^{-2}$. The MA reaches the extremely high value of 455 A g_{Ir}^{-1} for the 30 wt% catalyst, while for the other loadings MAs in the range 390–420 A g_{Ir}^{-1} are determined.

It is here important to stress that carbon black is not suitable as a support for OER catalysts, given the high operating cell potential in PEMWEs. Nevertheless, for the relatively short exposition to high potentials during the electrochemical characterization as employed in this work, we consider the contribution of the carbon oxidation to the measured overall current as negligible. To confirm this, we performed a reference test where carbon black was drop cast on the RDE tip. The carbon black ink was prepared following the same procedure used for all other materials described in this work. The amount was instead chosen to match the loading of carbon of Ir/C 30 wt%. The results reported in the SI (Figure S12) clearly indicate that the current contribution from carbon oxidation at the reference potential of 1.5 V_{RHE} can be neglected, and the measured overall current can be taken as OER rate. Similar conclusions were previously reported in literature when catalysts based on Pt NPs supported on carbon where investigated with differential electrochemical mass spectrometry (DEMS) to assess the stability of carbon at high voltages and the effect of the noble metal on the stability of the carbon during electrocatalytic processes [52,53]. It was showed that bare carbon indeed undergoes significant degradation during the first excursion to high voltages (above 1.5 V_{RHE}) but this process turns to a negligible current during all subsequent exposures to high potentials, as long as voltages higher than 1.0 V_{RHE} were employed [52]. If the lower voltage limit was maintained above 1.0 V_{RHE}, no significant deviation in carbon degradation could be detected even in presence of Pt NPs [53]. This does not imply that carbon is a suitable support material for technical water electrolysis, but that carbon can be used as model support to study the OER. In a previous work we have already reported that colloidal Ir NPs could be employed to prepare catalysts supported on the more electrochemically inert metal oxides, such as TiO_2, with values of MA higher than 200 A g_{Ir}^{-1} and SA of 180 $\mu A\ cm_{Ir}^{-2}$, a value that is very close to those reported in this work [54]. However, the rather low specific surface area and inhomogeneous morphology of such supports did not make them suitable candidates to assess the full theoretical potential of small colloidal Ir NPs. Therefore carbon was chosen as a proof-of-concept support material for investigating the importance of dispersion for OER catalysts.

Addressing the difference between the electrochemical performance of the Ir/C_{MeOH} and Ir/C_{EtOH} catalysts and the general implications for the synthesis of supported catalysts based on the colloidal approach, is important to point out once more that the colloidal stability of the NPs in the solvent is not the only aspect that needs consideration. As mentioned above, the as synthesized Ir NPs in MeOH are more stable than in EtOH (Table S4). The dispersibility of the carbon support, however, is significantly better in EtOH. To demonstrate that the dispersibility of the support not necessarily leads to limitations of the colloidal approach, we prepared a new set of catalysts by mixing Ir NPs prepared in MeOH and carbon support dispersed in EtOH. For this experiment, we took care to work with an excess of EtOH relative to MeOH. Thus, we avoided experiencing the same issues faced by pure MeOH-based catalysts. We observed nearly the same ECSA values as for the catalysts prepared solely in EtOH, e.g., 219 $m^2\ g_{Ir}^{-1}$ for the sample with 70 wt% (Figure S13). This experiment demonstrates that the dispersion of support and active phase can be optimized independently using different solvents that are compatible.

4. Conclusions

Three different strategies for preparing carbon supported Ir catalysts for the OER were compared, i.e. the surfactant-free colloidal polyol synthesis using EG and the recently introduced Co4Cat approach employing low-boiling point mono-alcohols. All three methods are suitable for preparing carbon supported OER catalysts with high initial activity. The main advantage of the surfactant-free synthesis as compared to other colloidal methods is that the supported catalysts can be used as prepared since the Ir NPs are not covered by stabilizing polymers such as polyvinylpyrrolidone (PVP) [15,17]. However, our results clearly show that the catalysts prepared by the polyol synthesis suffer from a material loss during the flocculation and redispersion steps required to remove the solvent. Despite the same particle size as in the Co4Cat approach, the ECSA is significantly reduced. Using mono-alcohols like MeOH and EtOH for preparation of the NPs and dispersion of the support, the solvent can be simply evaporated and recovered. This approach does not only generate significantly less waste; it also avoids loss of precious Ir metal. Furthermore, it is demonstrated that for obtaining finely dispersed Ir NPs onto a support material, not only the colloidal NP stability is important, but the dispersion of the support material in the solvent as well. In this regard, the colloidal approach is highly flexible as different solvents can be used for the NP synthesis and the support dispersion. Using carbon supports, such an optimization leads to OER catalysts with outstanding initial performance in a large range of metal loadings. The approach is flexible with regard to different support materials that are more relevant than carbon for technical applications, which will be studied in future work. To date, several metal oxides have been tested as possible candidates as support material and Sb-, In- and F-doped tin oxides are currently considered as the most promising [49,55]. They present decent conductivity and stability but are not completely inert under OER conditions [56]. Our work shows that covering these support with a monolayer of Ir NPs without agglomeration and decrease in the ECSA could be a possible strategy to improve the long-term stability of the catalysts.

Declaration of Competing Interest

The authors declare that they have no known competing financial interests or personal relationships that could have appeared to influence the work reported in this paper.

Acknowledgments

This work was supported by the Swiss National Science Foundation (SNSF) via the project No. 200021_184742. J.Q. acknowledges the European Union's Horizon 2020 research and innovation program under the Marie Skłodowska-Curie grant agreement No. 840523 (CoSolCat). The authors thank J.J.K.Kirkensgaard, University of Copenhagen, for this help on SAXS data acquisition as well as the Niels Bohr institute, University of Copenhagen, for access to equipment and S.B.Simonsen, Technical University of Denmark, for his help on HRTEM data acquisition.

Appendix A. Supplementary material

Supplementary data to this article can be found online at https://doi.org/10.1016/j.jcat.2021.07.004.

References

[1] G.L. Chiarello, M.H. Aguirre, E. Selli, Hydrogen production by photocatalytic steam reforming of methanol on noble metal-modified TiO_2, J. Catal. 273 (2) (2010) 182–190, https://doi.org/10.1016/j.jcat.2010.05.012.
[2] M. Ni, D.Y.C. Leung, M.K.H. Leung, A review on reforming bio-ethanol for hydrogen production, Int. J. Hydrogen Energy 32 (15) (2007) 3238–3247, https://doi.org/10.1016/j.ijhydene.2007.04.038.
[3] J.R. Rostrup-Nielsen, J. Sehested, J.K. Nørskov, Hydrogen and synthesis gas by steam- and CO_2 reforming, Adv. Catal. 47 (2002) 65–139, https://doi.org/10.1016/S0360-0564(02)47006-X.
[4] C. Smith, A.K. Hill, L. Torrente-Murciano, Current and future role of haber-bosch ammonia in a carbon-free energy landscape, Energy Environ. Sci. 13 (2) (2020) 331–344, https://doi.org/10.1039/c9ee02873k.
[5] C.C.L. McCrory, S. Jung, I.M. Ferrer, S.M. Chatman, J.C. Peters, T.F. Jaramillo, Benchmarking hydrogen evolving reaction and oxygen evolving reaction electrocatalysts for solar water splitting devices, J. Am. Chem. Soc. 137 (13) (2015) 4347–4357, https://doi.org/10.1021/ja510442p.
[6] C.C.L. McCrory, S. Jung, J.C. Peters, T.F. Jaramillo, Benchmarking heterogeneous electrocatalysts for the oxygen evolution reaction, J. Am. Chem. Soc. 135 (45) (2013) 16977–16987, https://doi.org/10.1021/ja407115p.
[7] I. Katsounaros, S. Cherevko, A.R. Zeradjanin, K.J.J. Mayrhofer, Oxygen electrochemistry as a cornerstone for sustainable energy conversion, Angew. Chemie Int. Ed. 53 (1) (2014) 102–121, https://doi.org/10.1002/anie.v53.110.1002/anie.201306588.
[8] T. Reier, M. Oezaslan, P. Strasser, Electrocatalytic oxygen evolution reaction (OER) on Ru, Ir, and Pt catalysts: a comparative study of nanoparticles and bulk materials, ACS Catal. 2 (8) (2012) 1765–1772, https://doi.org/10.1021/cs3003098.
[9] S. Siracusano, N. Hodnik, P. Jovanovic, F. Ruiz-Zepeda, M. Šala, V. Baglio, A.S. Aricò, New insights into the stability of a high performance nanostructured catalyst for sustainable water electrolysis, Nano Energy 40 (April) (2017) 618–632, https://doi.org/10.1016/j.nanoen.2017.09.014.
[10] M. Carmo, D.L. Fritz, J. Mergel, D. Stolten, A comprehensive review on PEM water electrolysis, Int. J. Hydrogen Energy 38 (12) (2013) 4901–4934, https://doi.org/10.1016/j.ijhydene.2013.01.151.
[11] M. Bernt, H.A. Gasteiger, Influence of ionomer content in IrO_2/TiO_2 electrodes on PEM water electrolyzer performance, J. Electrochem. Soc. 163 (11) (2016) F3179–F3189, https://doi.org/10.1149/2.0231611jes.
[12] J. Speder, A. Zana, I. Spanos, J.J.K. Kirkensgaard, K. Mortensen, M. Hanzlik, M. Arenz, Comparative degradation study of carbon supported proton exchange membrane fuel cell electrocatalysts – the influence of the platinum to carbon ratio on the degradation rate, J. Power Sources 261 (2014) 14–22, https://doi.org/10.1016/j.jpowsour.2014.03.039.
[13] J. Quinson, M. Inaba, S. Neumann, A.A. Swane, J. Bucher, S.B. Simonsen, L. Theil Kuhn, J.J.K. Kirkensgaard, K.M.Ø. Jensen, M. Oezaslan, S. Kunz, M. Arenz, Investigating particle size effects in catalysis by applying a size-controlled and surfactant-free synthesis of colloidal nanoparticles in alkaline ethylene glycol: case study of the oxygen reduction reaction on Pt, ACS Catal. 8 (7) (2018) 6627–6635, https://doi.org/10.1021/acscatal.8b0069410.1021/acscatal.8b00694.s001.
[14] J. Speder, A. Zana, I. Spanos, J.J.K. Kirkensgaard, K. Mortensen, M. Arenz, On The influence of the Pt to carbon ratio on the degradation of high surface area carbon supported PEM fuel cell electrocatalysts, Electrochem. Commun. 34 (2013) 153–156, https://doi.org/10.1016/j.elecom.2013.06.001.
[15] J.A. Arminio-Ravelo, J. Quinson, M.A. Pedersen, J.J.K. Kirkensgaard, M. Arenz, M. Escudero-Escribano, Synthesis of iridium nanocatalysts for water oxidation in acid: effect of the surfactant, ChemCatChem 12 (5) (2020) 1282–1287, https://doi.org/10.1002/cctc.v12.510.1002/cctc.201902190.
[16] J. Quinson, S. Kunz, M. Arenz, Beyond active site design: a surfactant-free toolbox approach for optimised supported nanoparticle catalysts, ChemCatChem cctc.202001858 (2021), https://doi.org/10.1002/cctc.202001858.
[17] Y. Wang, J. Ren, K. Deng, L. Gui, Y. Tang, Preparation of tractable platinum, rhodium, and ruthenium nanoclusters with small particle size in organic media, Chem. Mater. 12 (6) (2000) 1622–1627, https://doi.org/10.1021/cm0000853.
[18] J. Quinson, S. Neumann, T. Wannmacher, L. Kacenauskaite, M. Inaba, J. Bucher, F. Bizzotto, S.B. Simonsen, L. Theil Kuhn, D. Bujak, A. Zana, M. Arenz, S. Kunz, Colloids for catalysts: a concept for the preparation of superior catalysts of industrial relevance, Angew. Chemie Int. Ed. 57 (38) (2018) 12338–12341, https://doi.org/10.1002/anie.201807450.
[19] M. Inaba, J. Quinson, M. Arenz, PH matters: the influence of the catalyst ink on the oxygen reduction activity determined in thin film rotating disk electrode measurements, J. Power Sources 353 (2017) 19–27, https://doi.org/10.1016/j.jpowsour.2017.03.140.
[20] F. Bizzotto, J. Quinson, A. Zana, J.J.K. Kirkensgaard, A. Dworzak, M. Oezaslan, M. Arenz, Ir nanoparticles with ultrahigh dispersion as oxygen evolution reaction (OER) catalysts: Synthesis and activity benchmarking, Catal. Sci. Technol. 9 (22) (2019) 6345–6356, https://doi.org/10.1039/C9CY01728C.
[21] S.M. Alia, K.E. Hurst, S.S. Kocha, B.S. Pivovar, Mercury underpotential deposition to determine iridium and iridium oxide electrochemical surface areas, J. Electrochem. Soc. 163 (11) (2016) F3051–F3056, https://doi.org/10.1149/2.0071611jes.
[22] T. Zemb, P. Lindner, Neutron, X-Rays and Light. Scattering Methods Applied to Soft Condensed Matter, 1st Editio.; Zemb, T., Lindner, P., Eds.; Elsevier, 2002.
[23] S. Alinejad, J. Quinson, J. Schröder, J.J.K. Kirkensgaard, M. Arenz, Carbon-supported platinum electrocatalysts probed in a gas diffusion setup with alkaline environment: how particle size and mesoscopic environment influence the degradation mechanism, ACS Catal. 10 (21) (2020) 13040–13049, https://doi.org/10.1021/acscatal.0c0318410.1021/acscatal.0c03184.s001.
[24] J. Schröder, J. Quinson, J.K. Mathiesen, J.J.K. Kirkensgaard, S. Alinejad, V.A. Mints, K.M.∅. Jensen, M. Arenz, A new approach to probe the degradation of fuel cell catalysts under realistic conditions: combining tests in a gas diffusion electrode setup with small angle X-ray scattering, J. Electrochem. Soc. 167 (13) (2020) 134515, https://doi.org/10.1149/1945-7111/abbdd2.
[25] J. Quinson, S. Neumann, L. Kacenauskaite, J. Bucher, J.J.K. Kirkensgaard, S.B. Simonsen, L. Theil Kuhn, A. Zana, T. Vosch, M. Oezaslan, S. Kunz, M. Arenz, Solvent-dependent growth and stabilization mechanisms of surfactant-free colloidal Pt nanoparticles, Chem. - A Eur. J. 26 (41) (2020) 9012–9023, https://doi.org/10.1002/chem.v26.4110.1002/chem.202001553.
[26] P. Lettenmeier, J. Majchel, L. Wang, V.A. Saveleva, S. Zafeiratos, E.R. Savinova, J. J. Gallet, F. Bournel, A.S. Gago, K.A. Friedrich, Highly active nano-sized iridium catalysts: synthesis and operando spectroscopy in a proton exchange membrane electrolyzer, Chem. Sci. 9 (14) (2018) 3570–3579, https://doi.org/10.1039/c8sc00555a.
[27] A. Hartig-Weiss, M. Miller, H. Beyer, A. Schmitt, A. Siebel, A.T.S. Freiberg, H.A. Gasteiger, H.A. El-Sayed, Iridium oxide catalyst supported on antimony-doped tin oxide for high oxygen evolution reaction activity in acidic media, ACS Appl. Nano Mater. 3 (3) (2020) 2185–2196, https://doi.org/10.1021/acsanm.9b02230.
[28] M.L. Cui, Y.S. Chen, Q.F. Xie, D.P. Yang, M.Y. Han, Synthesis, properties and applications of noble metal iridium nanomaterials, Coord. Chem. Rev. 387 (2019) 450–462, https://doi.org/10.1016/j.ccr.2018.12.008.
[29] J. Speder, L. Altmann, M. Roefzaad, M. Bäumer, J.J.K. Kirkensgaard, K. Mortensen, M. Arenz, Pt based PEMFC catalysts prepared from colloidal particle suspensions – a toolbox for model studies, Phys. Chem. Chem. Phys. 15 (10) (2013) 3602, https://doi.org/10.1039/c3cp50195g.
[30] S. Neumann, J. Schröder, F. Bizzotto, M. Arenz, A. Dworzak, M. Oezaslan, M. Bäumer, S. Kunz, Halide-induced leaching of Pt nanoparticles – manipulation of particle size by controlled ostwald ripening, ChemNanoMat 5 (4) (2019) 462–471, https://doi.org/10.1002/cnma.v5.410.1002/cnma.201800550.
[31] J. Quinson, L. Kacenauskaite, J. Bucher, S.B. Simonsen, L. Theil Kuhn, M. Oezaslan, S. Kunz, M. Arenz, Controlled synthesis of surfactant-free water-dispersible colloidal platinum nanoparticles by the Co4Cat process, ChemSusChem 12 (6) (2019) 1229–1239, https://doi.org/10.1002/cssc.v12.610.1002/cssc.201802897.
[32] J. Quinson, J.K. Mathiesen, J. Schröder, A. Dworzak, F. Bizzotto, A. Zana, S.B. Simonsen, L. Theil Kuhn, M. Oezaslan, K.M.Ø. Jensen, M. Arenz, Teaching old precursors new tricks: fast room temperature synthesis of surfactant-free colloidal platinum nanoparticles, J. Colloid Interface Sci. 577 (2020) 319–328, https://doi.org/10.1016/j.jcis.2020.05.078.
[33] J. Quinson, J. Bucher, S.B. Simonsen, L.T. Kuhn, S. Kunz, M. Arenz, Monovalent alkali cations: simple and eco-friendly stabilizers for surfactant-free precious metal nanoparticle colloids, ACS Sustain. Chem. Eng. 7 (16) (2019) 13680–13686, https://doi.org/10.1021/acssuschemeng.9b0068110.1021/acssuschemeng.9b00681.s001.
[34] M.C. Figueiredo, A. Santasalo-Aarnio, F.J. Vidal-Iglesias, J. Solla-Gullón, J.M. Feliu, K. Kontturi, T. Kallio, Tailoring properties of platinum supported catalysts by irreversible adsorbed adatoms toward ethanol oxidation for direct ethanol fuel cells, Appl. Catal. B Environ. 140–141 (2013) 378–385, https://doi.org/10.1016/j.apcatb.2013.04.038.
[35] X. Xia, L. Figueroa-Cosme, J. Tao, H.C. Peng, G. Niu, Y. Zhu, Y. Xia, Facile synthesis of iridium nanocrystals with well-controlled facets using seed-mediated growth, J. Am. Chem. Soc. 136 (31) (2014) 10878–10881, https://doi.org/10.1021/ja505716v.
[36] M. Gliech, M. Klingenhof, M. Görlin, P. Strasser, Supported metal oxide nanoparticle electrocatalysts: how immobilization affects catalytic

performance, Appl. Catal. A Gen. 568 (August) (2018) 11–15, https://doi.org/10.1016/j.apcata.2018.09.023.
[37] A. Zana, J. Speder, N.E.A. Reeler, T. Vosch, M. Arenz, Investigating the corrosion of high surface area carbons during start/stop fuel cell conditions: a Raman study, Electrochim. Acta 114 (2013) 455–461, https://doi.org/10.1016/j.electacta.2013.10.097.
[38] A. Zana, J. Speder, M. Roefzaad, L. Altmann, M. Bäumer, M. Arenz, Probing degradation by IL-TEM: the influence of stress test conditions on the degradation mechanism, J. Electrochem. Soc. 160 (6) (2013) F608–F615, https://doi.org/10.1149/2.078306jes.
[39] J. Speder, L. Altmann, M. Bäumer, J.J.K. Kirkensgaard, K. Mortensen, M. Arenz, The particle proximity effect: from model to high surface area fuel cell catalysts, RSC Adv. 4 (29) (2014) 14971, https://doi.org/10.1039/c4ra00261j.
[40] M. Bernt, A. Hartig-Weiß, M.F. Tovini, H.A. El-Sayed, C. Schramm, J. Schröter, C. Gebauer, H.A. Gasteiger, Current challenges in catalyst development for PEM water electrolyzers, Chemie-Ingenieur-Technik 92 (1-2) (2020) 31–39, https://doi.org/10.1002/cite.v92.1-210.1002/cite.201900101.
[41] J. Speder, A. Zana, M. Arenz, The colloidal tool-box approach for fuel cell catalysts : systematic study of perfluorosulfonate-ionomer impregnation and Pt Loading. 262 (2016) 82–89.
[42] D.J.S. Sandbeck, N.M. Secher, M. Inaba, J. Quinson, J.E. Sørensen, J. Kibsgaard, A. Zana, F. Bizzotto, F.D. Speck, M.T.Y. Paul, A. Dworzak, C. Dosche, M. Oezaslan, I. b. Chorkendorff, M. Arenz, S. Cherevko, The dissolution dilemma for low Pt loading polymer electrolyte membrane fuel cell catalysts, J. Electrochem. Soc. 167 (16) (2020) 164501, https://doi.org/10.1149/1945-7111/abc767.
[43] J.C. Jiménez-García, J.A. Olmos-Asar, E.E. Franceschini, M.M. Mariscal, electrochemical area of graphene-supported metal nanoparticles from an atomistic approach, J. Appl. Electrochem. 50 (4) (2020) 421–429, https://doi.org/10.1007/s10800-020-01399-z.
[44] H.-S. Oh, H.N. Nong, T. Reier, M. Gliech, P. Strasser, Oxide-supported Ir nanodendrites with high activity and durability for the oxygen evolution reaction in acid PEM water electrolyzers, Chem. Sci. 6 (6) (2015) 3321–3328, https://doi.org/10.1039/C5SC00518C.
[45] E. Oakton, D. Lebedev, M. Povia, D.F. Abbott, E. Fabbri, A. Fedorov, M. Nachtegaal, C. Copéret, T.J. Schmidt, IrO_2-TiO_2: a high-surface-area, active, and stable electrocatalyst for the oxygen evolution reaction, ACS Catal. 7 (4) (2017) 2346–2352, https://doi.org/10.1021/acscatal.6b03246.
[46] H.N. Nong, L. Gan, E. Willinger, D. Teschner, P. Strasser, IrOx core-shell nanocatalysts for cost- and energy-efficient electrochemical water splitting, Chem. Sci. 5 (8) (2014) 2955–2963, https://doi.org/10.1039/C4SC01065E.
[47] Y. Lee, J. Suntivich, K.J. May, E.E. Perry, Y. Shao-Horn, Synthesis and activities of rutile IrO_2 and RuO_2 nanoparticles for oxygen evolution in acid and alkaline solutions, J. Phys. Chem. Lett. 3 (3) (2012) 399–404, https://doi.org/10.1021/jz2016507.
[48] H.-S. Oh, H.N. Nong, T. Reier, A. Bergmann, M. Gliech, J. Ferreira de Araújo, E. Willinger, R. Schlögl, D. Teschner, P. Strasser, Electrochemical catalyst-support effects and their stabilizing role for IrO x nanoparticle catalysts during the oxygen evolution reaction, J. Am. Chem. Soc. 138 (38) (2016) 12552–12563, https://doi.org/10.1021/jacs.6b0719910.1021/jacs.6b07199.s001.
[49] D. Lebedev, C. Copéret, Small, narrowly distributed iridium nanoparticles supported on indium tin oxide for efficient anodic water oxidation, ACS Appl. Energy Mater. 2 (1) (2019) 196–200, https://doi.org/10.1021/acsaem.8b0172410.1021/acsaem.8b01724.s001.
[50] C. Spöri, P. Briois, H.N. Nong, T. Reier, A. Billard, S. Kühl, D. Teschner, P. Strasser, Experimental activity descriptors for iridium-based catalysts for the electrochemical oxygen evolution reaction (OER), ACS Catal. 9 (8) (2019) 6653–6663, https://doi.org/10.1021/acscatal.9b0064810.1021/acscatal.9b00648.s001.
[51] D. Bernsmeier, M. Bernicke, R. Schmack, R. Sachse, B. Paul, A. Bergmann, P. Strasser, E. Ortel, R. Kraehnert, Oxygen evolution catalysts based on Ir–Ti Mixed oxides with templated mesopore structure: impact of Ir on activity and conductivity, ChemSusChem 11 (14) (2018) 2367–2374, https://doi.org/10.1002/cssc.v11.1410.1002/cssc.201800932.
[52] S.J. Ashton, M. Arenz, A DEMS study on the electrochemical oxidation of a high surface area carbon black, Electrochem. commun. 13 (12) (2011) 1473–1475, https://doi.org/10.1016/j.elecom.2011.09.024.
[53] N. Linse, L. Gubler, G.G. Scherer, A. Wokaun, The effect of platinum on carbon corrosion behavior in polymer electrolyte fuel cells, Electrochim. Acta 56 (22) (2011) 7541–7549, https://doi.org/10.1016/j.electacta.2011.06.093.
[54] A. Dutta, F. Bizzotto, J. Quinson, A. Zana, C.E. Morstein, M.A. Rahaman, A.C. López, M. Arenz, P. Broekmann, Catalyst development for water/CO_2 Co-electrolysis, Chim. Int. J. Chem. 73 (9) (2019) 707–713, https://doi.org/10.2533/chimia.2019.707.
[55] H. Ohno, S. Nohara, K. Kakinuma, M. Uchida, A. Miyake, S. Deki, H. Uchida, Remarkable mass activities for the oxygen evolution reaction at iridium oxide nanocatalysts dispersed on tin oxides for polymer electrolyte membrane water electrolysis, J. Electrochem. Soc. 164 (9) (2017) F944–F947, https://doi.org/10.1149/2.1101709jes.
[56] S. Geiger, O. Kasian, A.M. Mingers, K.J.J. Mayrhofer, S. Cherevko, Stability limits of tin-based electrocatalyst supports, Sci. Rep. 7 (1) (2017) 4595, https://doi.org/10.1038/s41598-017-04079-9.